

Dynamical friction in flattened systems: A numerical test of Binney's approach

Jorge Peñarrubia¹, Andreas Just¹, Pavel Kroupa^{2,3}

¹*Astronomisches Rechen-Institut, Mönchhofstrasse 12-14, D-69120 Heidelberg, Germany*

²*Institut für Theoretische Physik und Astrophysik, Universität Kiel, D-24098 Kiel, Germany*

³*Heisenberg Fellow*

1 October 2018

ABSTRACT

We carry out a set of self-consistent N -body calculations to investigate how important the velocity anisotropy in non-spherical dark-matter halos is for dynamical friction. For this purpose we allow satellite galaxies to orbit within flattened and live dark-matter haloes (DMHs) and compare the resulting orbit evolution with a semi-analytic code. This code solves the equation of motion of the same satellite orbits with mass loss and assumes the same DMH, but either employs Chandrasekhar's dynamical friction formula, which does not incorporate the velocity anisotropy, or Binney's description of dynamical friction in anisotropic systems. In the numerical and the two semi-analytic models the satellites are given different initial orbital inclinations and orbital eccentricities, whereas the parent galaxy is composed of a DMH with aspect ratio $q_h = 0.6$.

We find that Binney's approach successfully describes the overall satellite decay and orbital inclination decrease for the whole set of orbits, with an averaged discrepancy of less than 4 per cent in orbital radius during the first 3 orbits. If Chandrasekhar's expression is used instead, the discrepancy increases to 20 per cent. Binney's treatment therefore appears to provide a significantly improved treatment of dynamical friction in anisotropic systems.

The velocity anisotropy of the DMH velocity distribution function leads to a significant decrease with time of the inclination of non-polar satellite orbits. But at the same time it reduces the difference in decay times between polar and coplanar orbits evident in a flattened DMH when the anisotropic DMH velocity distribution function is not taken into account explicitly. Our N -body calculations furthermore indicate that polar orbits survive about 1.6 times longer than coplanar orbits and that the orbital eccentricity e remains close to its initial value if satellites decay slowly towards the galaxy centre. However, orbits of rapidly decaying satellites modelled with the semi-analytic code show a strong orbital *circularisation* ($\dot{e} < 0$) not present in the N -body computations.

Key words: stellar dynamics – methods: N-body simulations – methods: analytical – galaxies: kinematics and dynamics – galaxies: haloes – galaxies: dwarf

1 INTRODUCTION

According to current ideas galaxy formation began with small-amplitude Gaussian fluctuations at the early stages of the Universe. In hierarchical cosmological models, these fluctuations decrease with increasing scales, resulting first in the formation of low-mass objects that may merge, building up ever more massive structures. The shape and morphology of these objects are strongly dependent on the cosmological models, as one can conclude from N -body computations, although none of them predict spherical structures. The most successful hierarchical theory is the Cold Dark

Matter model (CDM). In this framework, aspherical bound dark matter haloes (DMHs) form as a result of gravitational clustering. The inclusion of gas dynamics in the CDM simulations (Udry & Martinet 1994, Dubinsky 1994) results to a Gaussian distribution of DMH density aspect ratios, $q_h \equiv c/a > 0$, where c and a are the minor and major axes of an oblate spheroid, of mean $\langle q_h \rangle = 1/2$ and dispersion equal to 0.15 (Dubinsky 1994). The degree of asphericity depends on the dark matter nature. For example, numerical computations based on the Λ CDM predict halo axis-ratios of $q_h \simeq 0.7$ (Bullock 2001), Hot Dark Matter models lead to haloes as round as $q_h = 0.8$ (Peebles 1993), whereas candi-

dates such as cold molecular gas (Pfenniger, Combes & Martinet 1994) and massive decaying neutrinos (Sciama 1990) may produce halo profiles as flattened as $q_h = 0.2$.

Observationally, measuring galaxy axis-ratio is complicated: (i) Stellar kinematics: Olling & Merrifield (2000) obtain an axis-ratio of $q_h \approx 0.8$ for our Galaxy. This method has the disadvantage of having access to information of our Galaxy only on small scales. (ii) The flying gas layer method (Olling 1996, Becquaert, Combes & Viallefond 1997): assuming that the HI emission comes from gas in hydrostatic equilibrium in galactic potentials axis-ratios as low as $q_h \approx 0.3$ are obtained for the galaxies NGC 891 and 4244, (iii) Warping gas layer: Hofner & Sparke (1994) find axis-ratios of approximately 0.7 for NGC 2903 and of $q_h \approx 0.9$ for NGC 2841, 3198, 4565 and 4013, (iv) X-ray isophotes: Boute & Canizares (1998) measure values of $q_h \approx 0.5$ for NGC 3923, 1332 and 720, (v) Polar ring galaxies: Arnaboldi et al. (1993) and Sackett et al. (1994) find an axis-ratio of $q_h \approx 0.3$ for NGC 4650A, 0.5 for the galaxy A0136-0801 and 0.6 for AM2020-504, (vi) Precessing dusty discs: Steinman-Cameron, Kormendy & Durisen (1992) measure an axis-ratio of 0.9 for the galaxy NGC 4753.

Another method, which we focus on here, is the analysis of satellite dynamics. There are two main different approaches to infer the halo shape from satellites. First, one may attempt to reproduce the observed tidal streams of Milky Way satellites as done, for instance, by Ibata et al. (2001) and Law et al. (2003) who, from measurements of velocity, position and structure of the Sagittarius dwarf galaxy, constrain the initial parameter space and, subsequently, calculate in detail the satellite mass loss. They find that the Milky Way halo potential cannot be more flattened than ≈ 0.8 , otherwise tidal streams would be too spread out and thick compared to the observations due to orbital precession. The second approach is a statistical study of satellite distribution around spiral galaxies. Holmberg (1969), Zaritsky & González (1999), Prada et al. (2003) and Sales & Lambas (2003) point out that satellites around disc galaxies are found more often aligned with the poles of the host galaxy, the so-called 'Holmberg effect', whereas Quinn & Goodmann (1986) find in their *N*-body study that the disc alone cannot account for the original statistical distribution of Holmberg's data. A remedy may be sought in the form of an extended non-spherical DMH. An anisotropic velocity (and mass) distribution will cause a satellite's orbit to align with the axes of the velocity ellipsoid of the host galaxy (Peñarrubia, Kroupa & Boily 2001, hereinafter PKB). In both schemes, a large number of numerical calculations is needed. In the former approach one should integrate several initial orbital parameters to find the best fit to the observed satellite characteristics, whereas in the latter approach an initial satellite sample should statistically reproduce the distributions expected from cosmological models of DMH formation. So far this is prohibitively time-expensive by means of any of the present *N*-body algorithms.

Several studies of satellite decay have shown that, in spherical systems, Chandrasekhar's dynamical friction (Chandrasekhar 1943) is accurate enough if the Coulomb logarithm remains as a free parameter to fit to the *N*-body data (e.g. van den Bosch et al. 1999, Colpi et al. 1999) since it also depends on the code parameters and the number of particles employed. For instance, Prugniel & Combes (1992)

and Whade & Donner (1996) find that dynamical friction is artificially increased due to numerical noise if the particle number is small. Semi-analytic methods that include Chandrasekhar's dynamical friction have been demonstrated to reproduce accurately the overall evolution of satellite galaxies (e.g. Velázquez & White 1999, Taylor & Babul 2001) and, therefore, represent a useful tool in order to carry out extensive studies with a large parameter space.

It is, however, still unclear how the inhomogeneity of the system distribution affects the satellite dynamics. Whereas Del Popolo (2003), Del Popolo & Gambera (1998) and Maoz (1993) show that dynamical friction increases the steeper the density profile is, Just & Peñarrubia (2002), following the theoretical scheme proposed by Binney (1977), hereinafter B77, find a negligible effect on the satellite orbit due to the symmetry of the inhomogeneous terms of dynamical friction.

Although Chandrasekhar's formula, which assumes an isotropic velocity distribution, reproduces accurately dynamical friction in spherical systems, an analytical study of Statler (1991) shows that in the case of Stäckel potentials the velocity anisotropy produce strong effects on the satellite orbit. The *N*-body computations of PKB confirm that Chandrasekhar's formula cannot account for the resulting satellite decay and evolution if the halo is flattened. The aim of this paper is to implement a semi-analytic scheme capable of tracking the dynamical evolution of substructures within flattened as well as spherical DMH's. With this purpose in mind, we implement in our code the analytic expressions of dynamical friction in systems with anisotropic velocity dispersions suggested by Binney (B77) and also used by Statler, which reproduces Chandrasekhar's for null anisotropy in velocity space. We as well compare the results of using Chandrasekhar's formula in axi-symmetric systems to determine the effects of the velocity anisotropy on satellite decay.

Section 2 introduces the models. In Section 3 we provide the code and galaxy parameters. We outline the dynamical friction approaches in Section 4 whereas in Section 6 we propose a simple technique to fit a free parameter (in our case the Coulomb logarithm) to the *N*-body data. In Section 7 we study how flattened DMHs affect satellite decay and calculate the degree of accuracy of Binney's formula. The paper concludes with Section 8.

2 GALAXY AND SATELLITE PARAMETERS

Our DMH model is that used by PKB to facilitate an inter-comparison of the disc and bulge effects on satellite decay (Peñarrubia 2003). Here we do not add the bulge and disc components in order to distill the dependency of dynamical friction on the velocity anisotropy in a spheroidal DMH.

In order to minimise computational time when constructing flattened DMHs, we apply a highly-efficient technique using multi-pole potential expansions to tailor the local velocity ellipsoid to the required morphology (Boily, Kroupa & Peñarrubia 2001). The MAGALIE code scales linearly with particle number and hence we can construct flattened DMHs consisting of $\gtrsim 10^6$ particles or more, in a short computational time.

Following PKB, the flattened DMH is described by a non-singular isothermal profile which, in cylindrical coordi-

nates (for $m^2[u = 0]$ see eq. 7), can be described as

$$\rho_h[m^2(0)] = \frac{M_h \alpha}{2\pi^{3/2} r_{\text{cut}}} \frac{\exp[-m^2(0)/r_{\text{cut}}^2]}{m^2(0) + \gamma^2}, \quad (1)$$

with $m^2(0) = R^2 + z^2/q_h^2$

M_h being the DMH mass, r_{cut} the cut-off radius and γ the core radius, and

$$\alpha \equiv \{1 - \sqrt{\pi}\beta \exp(\beta^2)[1 - \text{erf}(\beta)]\}^{-1} = \quad (2)$$

$$1 + \sqrt{\pi}\beta + (\pi - 2)\beta^2 + O(\beta^3)$$

where $\beta = \gamma/r_{\text{cut}} \lesssim 1/24$ in our calculations. For $\beta = 1/24$ we find $\alpha \simeq 1.076 \rightarrow 1$ already and hence thereafter we set $\alpha = 1$ in our analysis.

We use self-consistent King models (King 1966) to represent our dwarf galaxies. These models fit early-type dwarf galaxies (Binggeli et al. 1984). For a comparison with the work of PKB we adopt $c = \log_{10}(r_t/r_c) = 0.8$, where r_c and r_t are the core and tidal radii, respectively.

To construct the models we choose the satellite mass M_s and r_t . The tidal radius is determined by computing the density contrast, $\rho_s(r_t)/\overline{\rho_g}(r_a) \sim 3$, at the apo-centric distance ($r_a = 55$ kpc) at $t = 0$, $\overline{\rho_g}(r)$ being the averaged density of the galaxy (same procedure as Velázquez & White 1999). This guarantees that all satellite particles are bound at $t = 0$.

We employ the system of units of PBK, which refers to the parameters of the Milky Way disc. Adopting $M_d = R_d = G = 1$ and according to Bahcall, Smith & Soneira (1982), $M_d = 5.6 \times 10^{10} M_\odot$ and $R_d = 3.5$ kpc, the time and velocity units are, respectively, 1.3×10^7 yr and 262 kms^{-1} .

The values of the galaxy and the satellite parameters can be found in Table 1. The parent galaxy corresponds to the model G2 of PKB, with the difference that we remove the disc and bulge components here.

3 NUMERICAL CALCULATIONS

3.1 Code parameters

The numerical experiments were carried out by using the code SUPERBOX which is a highly efficient particle mesh-algorithm based on a leap-frog scheme (for a detailed description see Fellhauer et al. 2000). SUPERBOX has already been implemented in extensive studies of satellite disruption by Kroupa (1997), Klessen & Kroupa (1998) and PKB. The program calculates the accelerations using a high order NGP ('nearest grid point') force calculation scheme based on the second derivatives of the potential. A self-consistent system of several galaxies can be treated by forming sub-grids (3D 'boxes') which follow the motion of each galaxy. Each sub-grid has three levels of resolution, the two finest levels co-move with the galaxies allowing a high-resolution calculation of the forces acting on the particles, whereas the third one covers the local 'Universe'. The finest levels are centred on the density maximum of the galaxy, which is recomputed at every time-step.

The code parameters are those of PKB. In that paper a detailed description of the system and the grid structure is presented, whereas here we merely give a brief description of the N-body parameters. Our integration time step is 0.39

	Symbol	Value(ph.u)	Value (m.u)
DMH (H2)	N_h	1 400 000	
	M_h	$7.84 \times 10^{11} M_\odot$	14.00
	q_h	0.60	0.60
	γ	3.5 kpc	1.00
Satellite (S1)	r_{cut}	84.00 kpc	24.00
	N_s	40 000	
	M_s	$5.60 \times 10^9 M_\odot$	0.10
	$\Psi(0)/\sigma_0^2$	5.00	5.00
	r_c	0.67 kpc	0.19
	r_t	7.24 kpc	2.07
	c	1.03	1.03
	$\langle r \rangle$	1.64 kpc	0.47
	σ_0	60.30 kms^{-1}	0.23

Table 1. Primary galaxy and satellite models. The DMH has an aspect ratio $q_h = 0.6$. For the satellite model: $\Psi(0) = \Phi(r_t) - \Phi(0)$, $\Phi(0)$ are the central potential and $\Phi(r_t)$ the potential at the tidal radius (following the notation of Binney & Tremaine 1987); σ_0 is the velocity dispersion at the centre, and $\langle r \rangle$ the average radius of the satellite. The units are such that Ph.u. means 'physical units' and m.u. 'model units'. N_h and N_s are the number of particles used to represent the DMH and the satellite, respectively.

Myr which is about 1/40th the dynamical time of our satellite. We have three resolution zones, each with 64^3 grid-cells: (i) The inner grid covers out to 3 radial halo scale-lengths, providing a resolution of 350 pc per grid-cell. (ii) The middle grid covers the whole galaxy, with an extension of 24 halo scale-lengths (84 kpc), giving a resolution of 2.8 kpc per grid-cell. The satellite always orbits within this grid except at the very late stages of its evolution, avoiding cross-border effects (see Fellhauer et al. 2000) and (iii) The outermost grid extends to 348 kpc and contains the local universe, at a resolution of 11.6 kpc. As for the satellite grid-structure, the resolutions are 816 pc per grid-cell for the inner grid that extends to 24.48 kpc, 1.2 kpc per grid-cell for the middle grid which extends to 36 kpc, and 11.6 kpc per grid-cell for the outermost grid that covers the local universe.

The selection of grid parameters ensures the conservation of energy and angular momentum for satellites in isolation over times as long as our calculations to better than 1% for all the models.

3.2 Orbital parameters

The parameter space of satellite galaxies is extremely large. A complete survey should account for different satellite masses, apo-galacticon distances, orbital eccentricities and inclinations...etc. In this paper, we carry out a set of calculations selecting those parameters that best reflect the effects of the velocity dispersion anisotropy on satellite decay. These parameters are: (i) the initial orbital inclination (i), defined as the angle between the initial angular momentum vector of a satellite and the axis perpendicular to the axi-symmetry plane (selected as the z -axis). We expect orbital inclination to decrease in time as predicted by Binney.

Name	Gal. model	Sat. model	i	e	r_p [kpc]	r_a [kpc]
H2S100	H2	S1	0°	0.5	18	55
H2S130	H2	S1	30°	0.5	18	55
H2S145	H2	S1	45°	0.5	18	55
H2S160	H2	S1	60°	0.5	18	55
H2S190	H2	S1	90°	0.5	18	55
H2S100c	H2	S1	0°	0.3	30	55
H2S130c	H2	S1	30°	0.3	30	55
H2S145c	H2	S1	45°	0.3	30	55
H2S160c	H2	S1	60°	0.3	30	55
H2S190c	H2	S1	90°	0.3	30	55
H2S100e	H2	S1	0°	0.7	10	55
H2S130e	H2	S1	30°	0.7	10	55
H2S145e	H2	S1	45°	0.7	10	55
H2S160e	H2	S1	60°	0.7	10	55
H2S190e	H2	S1	90°	0.7	10	55

Table 2. The numerical experiments. The peri- and apo-galactica are r_p and r_a , respectively, and $e = (r_a - r_p)/(r_a + r_p)$ is the orbital eccentricity.

We note that all the calculations proceed with the same orbital sense, but this is not important since the halo is non-rotating. (ii) The satellite's initial orbital eccentricity, defined as $e = (r_a - r_p)/(r_a + r_p)$, where r_a, r_p are the apo- and peri-galacticon, respectively.

The parameters of the numerical experiments are listed in Table 2.

4 HALO DYNAMICAL FRICTION

Chandrasekhar's expression cannot explain some effects observed in N-body calculations of satellite decay within flattened haloes (PKB). Our aim is to check Binney's approximation (B77) for systems with anisotropic velocity dispersion.

For simplicity, we reproduce here the analytic formulæ employed throughout this study (for a detailed analysis of the friction force see Peñarrubia 2003 and Just & Peñarrubia 2002).

If the distribution function in velocity space is axisymmetric, the zeroth order specific friction force is (B77)

$$F_i = -\frac{2\sqrt{2\pi}\rho_h[m^2(0)]G^2M_s\sqrt{1-e_v^2}\ln\Lambda}{\sigma_R^2\sigma_z}B_Rv_i, \quad (3)$$

$$F_z = -\frac{2\sqrt{2\pi}\rho_h[m^2(0)]G^2M_s\sqrt{1-e_v^2}\ln\Lambda}{\sigma_R^2\sigma_z}B_zv_z,$$

where $i = x, y$ and (σ_R, σ_z) is the velocity dispersion ellipsoid of a Schwarzschild distribution in cylindrical coordinates with constant ellipticity $e_v^2 = 1 - (\sigma_z/\sigma_R)^2$, $\ln\Lambda$ is the Coulomb logarithm of the halo and

$$B_R = \int_0^\infty dq \frac{\exp(-\frac{v_R^2/2\sigma_R^2}{1+q} - \frac{v_z^2/2\sigma_R^2}{1-e_v^2+q})}{(1+q)^2(1-e_v^2+q)^{1/2}},$$

$$B_z = \int_0^\infty dq \frac{\exp(-\frac{v_R^2/2\sigma_R^2}{1+q} - \frac{v_z^2/2\sigma_R^2}{1-e_v^2+q})}{(1+q)(1-e_v^2+q)^{3/2}},$$

where (v_R, v_z) are the coordinates of the satellite velocity in this frame.

As Binney shows, a body with mass M_s will suffer a decrease of its orbital inclination whenever $B_z > B_R$ (oblate halo). If the orbit is either coplanar or polar, the inclination remains constant since, respectively, the perpendicular and the planar component of \mathbf{v} is zero. It is straight-forward to show that this expression reproduces Chandrasekhar's for $e_v = 0$,

$$\mathbf{F}_{\text{ch}} = -4\pi GM_s\rho_h[m^2(0)]\ln\Lambda \left[\text{erf}(X) - \frac{2X}{\sqrt{\pi}}e^{-X^2} \right] \frac{\mathbf{v}_s}{v_s^3}, \quad (4)$$

where $X = |\mathbf{v}_s|/\sqrt{2}\sigma$.

One important aspect to note is that both expressions of dynamical friction include here an anisotropic halo density, denoted by $\rho_h[m^2(0)] = \rho_h[R^2 + z^2/q_h^2]$ in cylindrical coordinates. This is the “local approximation” made here but we note that the derivation of eq. 4 assumes a uniform, infinitely extended background medium. In practice, the local approximation implies the only difference between both expressions to be the anisotropic terms of the velocity distribution.

5 THE SEMI-ANALYTICAL CODE

In order to analyse the accuracy of the analytic expressions of dynamical friction we have constructed a semi-analytic algorithm that solves the equation of motion of a point-mass satellite

$$\frac{d^2\mathbf{x}}{dt^2} = \mathbf{F}_g + \mathbf{F}_{\text{df}}, \quad (5)$$

where \mathbf{F}_g is the specific force from the parent galaxy and \mathbf{F}_{df} that due to dynamical friction (eqs. 3 or 4).

If the parent galaxy follows the fixed density profile of eq. (1), the specific force can be written in Cartesian coordinates (Chandrasekhar 1960) as

$$F_{g,i} = -2\pi Gx_i \int_0^\infty \frac{du}{(1+u)^2(1+e_h^2+u)^{1/2}} \rho_h[m^2(u)], \quad (6)$$

$$F_{g,z} = -2\pi Gz \int_0^\infty \frac{du}{(1+u)(1+e_h^2+u)^{3/2}} \rho_h[m^2(u)],$$

where $x_i = x, y$, the ellipticity of the galaxy is $e_h^2 \equiv 1 - q_h^2$, and

$$m^2(u) = \frac{R^2}{1+u} + \frac{z^2}{1-e_h^2+u}. \quad (7)$$

The algorithm employed to solve eq. (5) is based on the Bulirsch-Stoer method (for a complete description see Press et al. 1986), which provides high-accurate solutions with minimal computational effort. This method is based on an adaptive step-size scheme, thus, being ideal for systems with non-smooth potentials, as may be the case for satellites on highly eccentric orbits when disc and bulge components are included.

For calculating \mathbf{F}_{df} (eqs. 3 and 4) the Coulomb logarithm is treated as a free parameter to be fitted to the numerical orbits. The satellite mass $M_s(t)$ is obtained from the N-body data (see Section 7.1) and is treated as an input function. Numerical tests of orbits in a Keplerian potential show that energy and angular momentum are conserved to

10^{-8} and 10^{-9} per orbit, respectively, after choosing the accuracy of the Bulirsch-Stoer algorithm to be $\text{EPS} = 10^{-5}$. This value remains fixed for the calculations presented in this paper. An extensive description of our semi-analytic code can be found in Peñarrubia (2003).

6 DETERMINING THE COULOMB LOGARITHM

The Coulomb logarithm is usually fit to numerical data with the aim of reproducing the overall orbital evolution by means of semi-analytic algorithms (e.g. Fellhauer et al. 2000). This procedure may actually be considered as a ‘‘calibration’’ of the semi-analytic code, which must be done carefully if a detailed inter-comparison between different schemes of dynamical friction is desired. For that reason we present in what follows a method to describe the accuracy of the semi-analytic scheme.

One possible way to quantify similarity of two orbits is via the quantity

$$\chi^2 = \frac{1}{2k} \sum_{i=1}^{2k} [(\mathbf{r}_i - \mathbf{r}_{i,n})^2 + \sigma^2(r_0)(t_i - t_{i,n})^2], \quad (8)$$

\mathbf{r} being the satellite position vector at the peri- and apo-galactica and t the time at which the satellite passes by these points. The subindex n denotes the numerical values and $\sigma(r_0)$ the velocity dispersion of the DMH at the initial galacto-centre distance. The sum is over a given number of orbits k .

The definition of χ measures the divergence of the numerical and semi-analytical satellite position. The term $\sigma\Delta t$ allows for the possibility that the orbital periods differ during the evolution, which would lead to a secular deviation. By definition, χ is equivalent to the discrepancy between the numerical and semi-analytical position evolution per orbit. The selection of the maximum and minimum galacto-centre distances for comparison permits a direct control over the orbital eccentricity evolution, although the measure of χ can be extended to other points without loss of generality.

The value of k depends on the objectives of the study. For instance, if the aim is to find the best calibration for a large period of time, as it may be to reproduce the satellite decay in spiral galaxies, the k -value must include a number of periods large enough, so that the overall evolution of several satellite orbits can be reproduced with a single value of $\ln\Lambda$. In this paper, we limit our fit to the first satellite periods, namely, $k = 3, 4$, for which the differences between both approaches of dynamical friction can be clearly seen.

In Fig. 1 we plot χ for some of the experiments, concretely, those with inclinations 60° , 45° and 30° (rows), with eccentricities 0.3 , 0.5 and 0.7 (columns). For each model, the semi-analytic code is employed to generate the satellite orbit using Chandrasekhar's (dashed and dotted-dashed lines) and Binney's (full and dotted lines) formula to reproduce dynamical friction. This figure shows that Chandrasekhar's formula poorly describes the dependence of the satellite orbit with the initial inclination, leading to a wider dispersion of the Coulomb logarithm values (for this range of inclinations, between 30° and 60° , $\ln\Lambda \in [0.9, 2.8]$). If Binney's expression is used, the variation of $\ln\Lambda$ is highly reduced

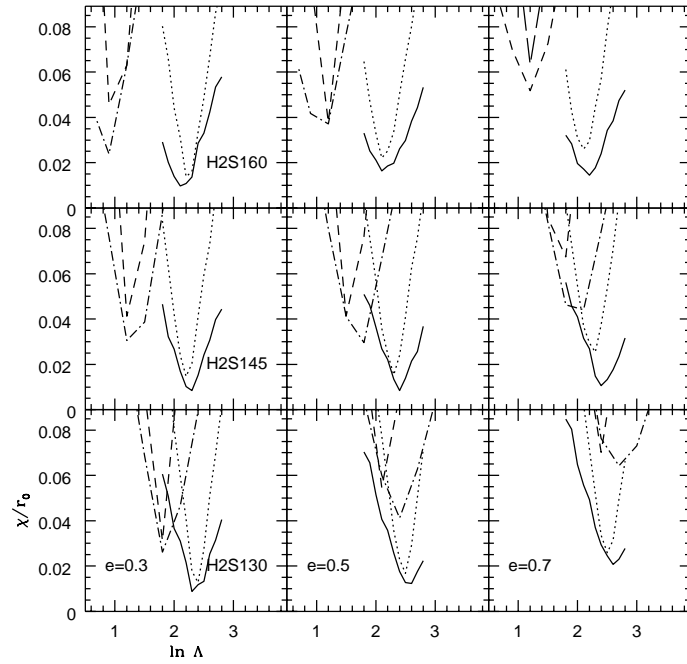


Figure 1. The parameter χ for different orbital eccentricities and inclinations. Dotted lines denote the first 4 orbits, whereas solid lines the first 3 orbits, in both cases using Binney's expressions for dynamical friction. Dashed and dot-dashed lines represent the results using Chandrasekhar's expression for $k = 4$ and 3 orbits, respectively. The χ values are normalised to the initial apo-galacticon distance $r_0 = 55$ kpc.

($\ln\Lambda \in [2.3, 2.5]$), which shows that this scheme provides a much better description of the effects of anisotropic velocity dispersion on satellite decay, independently of the orbital inclination. The variation range of the Coulomb logarithm becomes larger for a wider inclination spread, but χ barely presents a dependence on the satellite eccentricity if Binney's formula is applied.

If Chandrasekhar's approach is used, the Coulomb logarithm that leads to the best fit becomes smaller as the inclination increases. Since dynamical friction is proportional to $\ln\Lambda$, the use of the average value implies an overestimate of the force for low inclinations and *vice versa*. The final average,

$$(\chi/r_0) = \frac{1}{N_{\ln\Lambda}} \sum_{\ln\Lambda} \chi_i/r_0, \quad (9)$$

over the $N_{\ln\Lambda}$ numerical experiments of Table 2 is plotted in Fig. 2. This figure shows the large discrepancies produced by Chandrasekhar's expression if the fit is for a large range of orbital inclinations and eccentricities, as expected. The minima of the curves determine the values of $\ln\Lambda$ that lead to the best fits, which we summarise in Table 3. The values of χ_{\min} denote the average error during the first k orbits associated with the fit.

For the following analysis the value of the Coulomb logarithm implemented in our semi-analytic code will be found in Table 3. Looking at Fig. 1, we expect that Chandrasekhar's friction will lead to more accurate fits for low ($i \simeq 30^\circ$) than for high inclined orbits after fixing $\ln\Lambda = 2.2$.

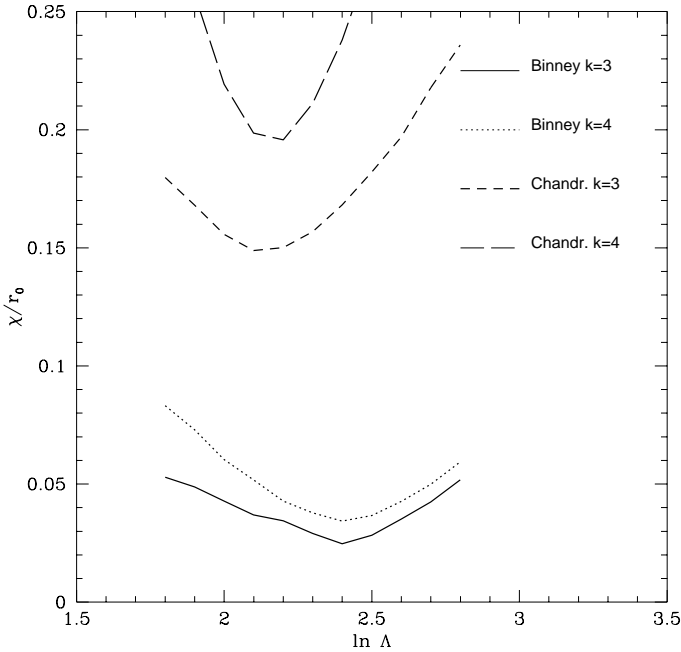


Figure 2. Average of the fitting parameters over the calculations of Table 2.

Friction	k	lnΛ	χ_{\min}/r_0	$\chi_{\min}/(k r_0)$
Binney	3	2.4	0.024	0.0080
	4	2.4	0.038	0.0095
Chandrasekhar	3	2.1	0.147	0.049
	4	2.2	0.193	0.048

Table 3. Results of the fitting procedure applied to the numerical calculations of Table 2 for both formulæ of dynamical friction. The fifth column gives relative deviation per orbit.

7 THE VELOCITY ANISOTROPY EFFECTS

In this Section, we discuss in more detail various aspects of satellite evolution.

7.1 Satellite mass loss

Tidal forces induce satellite mass loss. The satellite mass plays an important role in determining the ultimate fate of its evolution and survival (e.g. Velázquez & White 1999, Klessen & Kroupa 1998, Johnston et al. 1999). The value of $M_s(t)$ is treated as an input by the semi-analytical code, and is calculated using the self-consistent SUPERBOX code.

The mass remaining bound to the satellite, $M_s(t)$, is determined in the SUPERBOX calculations by computing the potential energy $\Phi_i < 0$ of each satellite particle presumed bound to the satellite, and its kinetic energy (T_i) in the satellite frame. Following PKB, particles with $E_i = T_i + m_s(\Phi_i + \Phi_{\text{ext}}) > 0$ are labelled unbound, where m_s is the mass of one satellite particle (all have the same mass) and

the potentials

$$\Phi_i = - \sum_{i \neq j} \frac{G m_s}{\sqrt{|r_i - r_j|^2 + \epsilon^2}}, \quad (10)$$

$$\Phi_{\text{ext}} = |\Phi_g(r_s)|,$$

the softening being $\epsilon \simeq 0.23 \text{ mu} = 0.8 \text{ kpc}$, which is the resolution of the inner grid focused on the satellite centre-of-density r_s , and Φ_g the galaxy potential at this point, neglecting the tidal terms. Thus, all the particles of a satellite are assumed to feel the same external potential, which is a useful and sufficiently accurate approximation, taking into account that most of the bound particles are located very close to this point.

Particles with $E_i > 0$ are removed and the procedure repeated until only negative energy particles are left. As Johnston et al (1999) show, the energy criterium permits one to distinguish those particles that, though unbound, remain in orbits inside the tidal radius, which will escape from the satellite after some orbital periods.

The mass is calculated each $\Delta t = 0.312 \text{ Gyr}$, so that the semi-analytic code interpolates the value for intermediate points at each time-step. The error is of the order of $\Delta M(t)/\Delta t$, going linearly with the mass loss. This means that the interpolation might introduce not negligible differences at times where the mass loss is significant (i.e late times of the satellite evolution). In this study we are not concerned in detail with the late phases of evolution.

In the right columns of Fig. 3a, b and c we plot the mass evolution for different orbits. Most of the satellites reach the inner most regions of the parent galaxy with a substantial fraction of their initial mass. A comparison of these curves with those of PKB (where a bulge and a disc component were included) shows that the baryonic subsystems of a galaxy induce a larger mass loss through tidal heating (e.g. Taylor & Babul 2001, Peñarrubia 2003). PKB observe in their numerical experiments that all satellites with $M_s = 0.1M_d$ and $r_0 = 55 \text{ kpc}$ are destroyed before the remaining bound part of the satellite reaches the central region of the galaxy.

7.2 Satellite decay

One of the most important effects of dynamical friction is the monotonic reduction of the orbital angular momentum and energy during the satellite's evolution that leads to a progressive decrease of the averaged galacto-centre distance. The computations carried out by PKB show a strong dependence of the decay time on the initial inclination that must be compared to analytic estimates.

In Fig. 3a, b and c we plot the radius evolution (left columns) for those models with initial $e = 0.5, 0.7$ and 0.3 , respectively. From this figure, we conclude that Binney's expression clearly produces more accurate results than Chandrasekhar's for the whole range of orbital inclinations. This result is not surprising due to the small dependence of the Coulomb logarithm on the inclination and eccentricity as shown in Fig. 1. Additionally, the value of $\ln \Lambda$ that produces the best fit for the first few orbits also succeeds in reproducing the decay time of the satellite.

PKB observe that coplanar satellites suffer larger friction than those following polar orbits, leading to survival

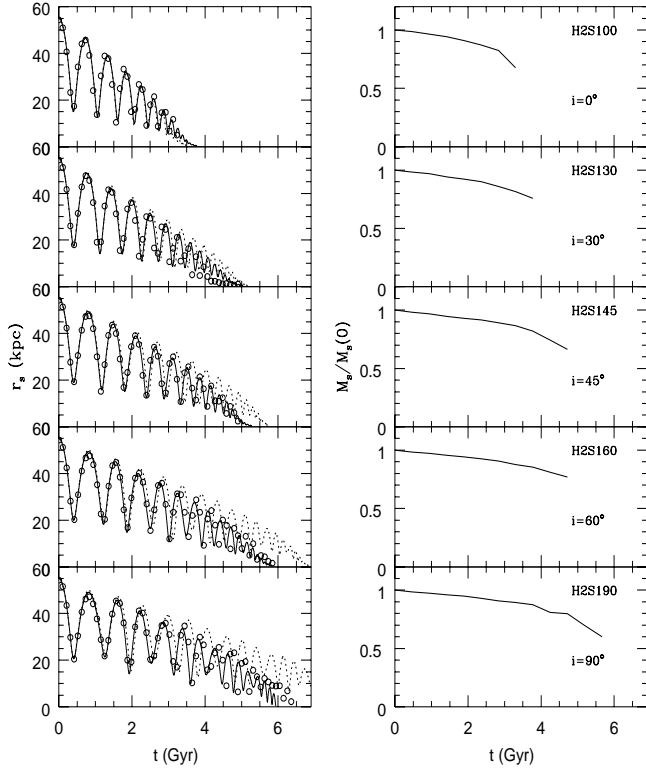


Figure 3. a: Radius and mass evolution for the models of Table 2 with initial $e = 0.5$. Open circles denote the numerical evolution, whereas full and dotted lines represent the data obtained from the semi-analytic code using, respectively, Binney's ($\ln \Lambda = 2.4$) and Chandrasekhar's ($\ln \Lambda = 2.2$) expressions to reproduce dynamical friction.

times 70% shorter. Due to the presence of a disc in their galaxy model, the contribution of the disc anisotropy on the decay differentiation as a function of the inclination cannot be directly measured. The calculations presented here (where the disc and bulge are removed) show survival times that range from 3.7 Gyr (coplanar orbits) to 6 Gyr (polar orbits), using the same orbital parameters and halo flattening as PKB. This implies a decay time difference of around 60% between polar and coplanar satellites, which indicates that the disc contribution might be of the order of 10%. The effects of the disc on the satellite orbit can be found in Peñarrubia (2003) and will be addressed in a following paper.

Depending on the symmetry of the halo distribution, one can observe the following effects:

- **Spherical mass distribution and isotropic velocity distribution:** Satellites orbiting systems with a spherical distribution function move on orbits that do not depend on their orientation with respect to the symmetry axis.

- **Flattened mass distribution and isotropic velocity distribution:** By means of the local approximation the value of dynamical friction is determined by the properties of the halo at the satellite's position, being reproduced by Chandrasekhar's formula. Our results indicate that the spatial asphericity leads to a strong differentiation of the satellite decay as a function of the orbital inclination.

- **Flattened mass distribution and anisotropic ve-**

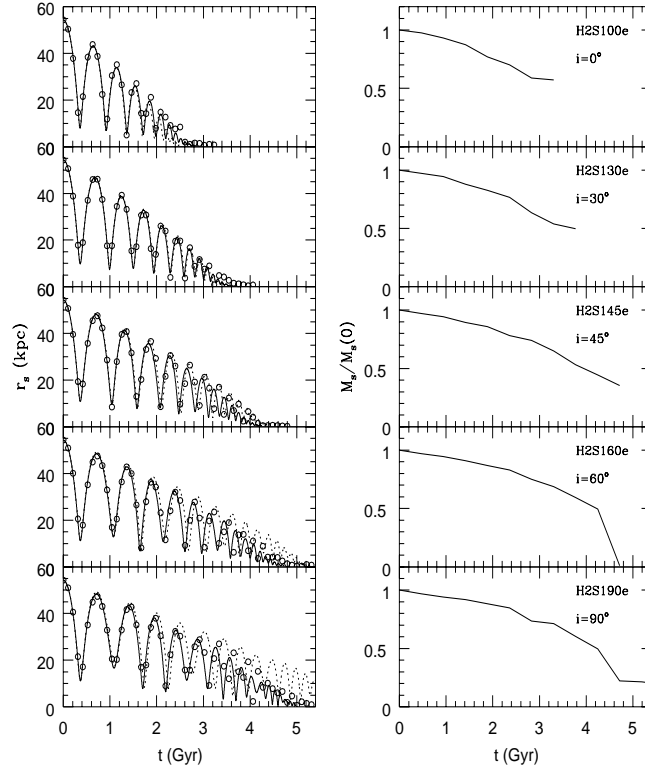


Figure 3 – continued b: As Fig. 3a for those satellites of Table 2 with initial $e = 0.7$. (Note that the time-axis has changed scale.)

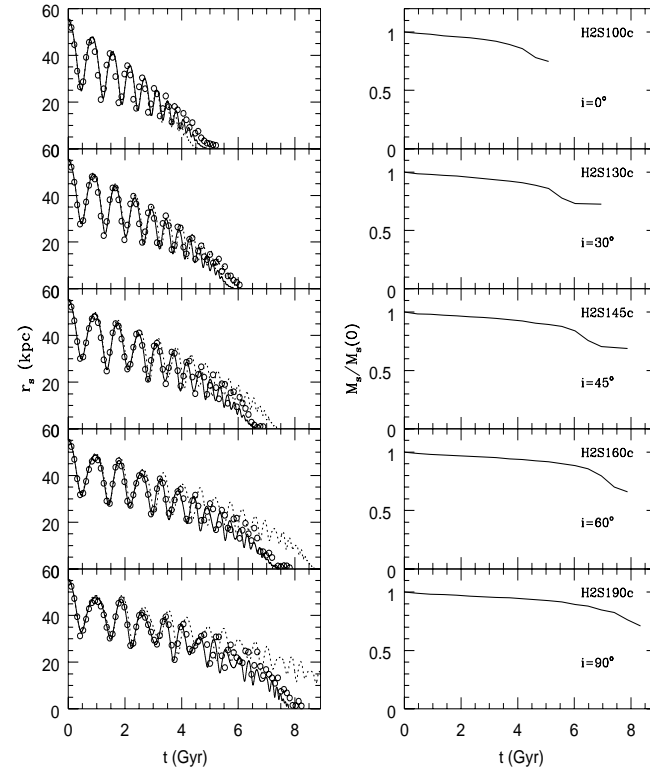


Figure 3 – continued c: As Fig. 3a for those satellites of Table 2 with initial $e = 0.3$. (Note that the time-axis has changed scale.)

locity distribution: The main influence of the velocity anisotropy on the satellite orbit is the secular reduction of the orbital inclination (see Subsection 7.3) and the reduction of the spatial anisotropy effects, which is equivalent to $B_R < B_z$ in Binney's formula (eq. 3, oblate systems). *Taking into account the velocity anisotropy explicitly thus reduces the difference in orbital decay times between satellites on polar and coplanar orbits.* As Fig. 3 shows, assuming an isotropic distribution in velocity space ($B_R = B_z$) or, equivalently, using Chandrasekhar's formula to reproduce dynamical friction, leads to an overestimation of dynamical friction for low inclined satellites and to an underestimation for those satellites following highly inclined orbits. This is due to the fact that the anisotropy leads to a reduced effective X for high inclined orbits yielding an enhanced friction force and vice versa for low inclination. This competes with the density effect due to the flattening, because highly inclined orbits have lower mean density along the orbit compared to lower inclination.

The evolution of the orbital radius of satellites with initial $e = 0.3, 0.7$ is plotted in Fig. 3b and c. As we can observe, Binney's approximation reproduces accurately the overall radius evolution independent of the initial eccentricity and orbital inclination.

7.3 Evolution of the orbital inclination and eccentricity

Orbits in non-spherical systems have inclinations ($i \equiv \arccos[L_z/L]$) that do not remain constant but suffer peridical oscillations due to *nutation*. In addition, the orbital plane precesses at a constant rate. Once the initial conditions are fixed, the amplitude and frequency of nutation and the precession rate remain constant if the friction force is removed from the equations of motion, whereas, if implemented, nutation and precession vary according to the angular momentum and radial distance evolution. Our interest focuses now on the effects induced by the velocity anisotropy on the satellite inclination during the orbit.

Binney (B77) predicts a progressive reduction of i due to dynamical friction if the velocity dispersion ellipsoid is axi-symmetric (σ_R, σ_z) and $\sigma_R > \sigma_z$. By symmetry, the inclination decrease will not occur if the orbits are either coplanar ($i = 0^\circ$) or polar ($i = 90^\circ$).

The inclination evolution of models with $e = 0.5$ is plotted in Fig. 4 (left column), where dotted lines denote the numerical data and solid and dashed lines the semi-analytic evolution if dynamical friction is modelled by Binney's and Chandrasekhar's formulæ, respectively. This Figure shows the reduction of the mean value of i predicted by Binney and observed by PKB in their numerical experiments. After the satellite has sunk to the inner most region of the halo, the inclinations are as low as $10^\circ - 20^\circ$ independent of their initial value. This large decrease of i is well reproduced by Binney's expression, although the nutation process shows discrepancies with the numerical result, which is connected with the not exact reproduction of the orbit. Despite the accurate description of the overall decay process, this orbital mismatch is also observed when applying Chandrasekhar's expression in spherical systems (see Just & Peñarrubia 2002). The fig-

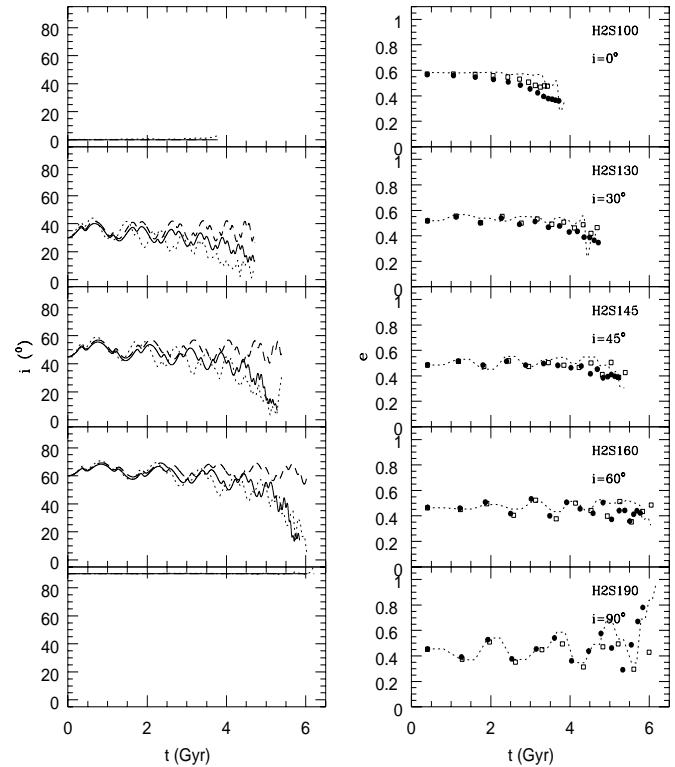


Figure 4. a: Inclination and eccentricity evolution for the models of Table 2 with $e = 0.5$. Left column: Dotted lines represent the N-body inclination evolution, full and dashed lines denote the use of Binney's and Chandrasekhar's equations, respectively. Right column: Numerical (dotted lines) against semi-analytical eccentricity evolution. Solid circles and open squares denote the implementation of Binney's and Chandrasekhar's expressions in the semi-analytic code, respectively. We note that, for clarity, the semi-analytic values of e are only plotted at the apo-centres.

ure also confirms that the orbital inclination of coplanar and polar satellites remains constant.

If dynamical friction is modelled by Chandrasekhar's formula, i.e the velocity distribution is assumed to be isotropic, the averaged value of i does not change during the orbit, which contradicts the numerical results. Thus, while the difference between the survival times of polar and coplanar orbits is larger for flattened DMHs treated with Chandrasekhar's dynamical friction formula (Fig. 3), taking into account the DMH anisotropic velocity distribution function explicitly via Binney's formulæ leads to an increase with time of the anisotropy of the satellite distribution due to the kinematical coupling of the satellites to the DMH velocity field. This clearly agrees with the fully self-consistent N -body computations reported here.

In Fig. 4b and 4c (left columns) we plot the comparison for models with $e = 0.7, 0.3$, respectively. The results show barely a dependence on the eccentricity. It is interesting to note that, independently of e , orbits that are neither coplanar nor polar present large drops of the mean value of i . After the satellite sinks to the centre, the final orbital inclination lies in between $10-20^\circ$ for all the models.

We must emphasise the accuracy of Binney's formula in describing correctly the inclination decrease that satel-

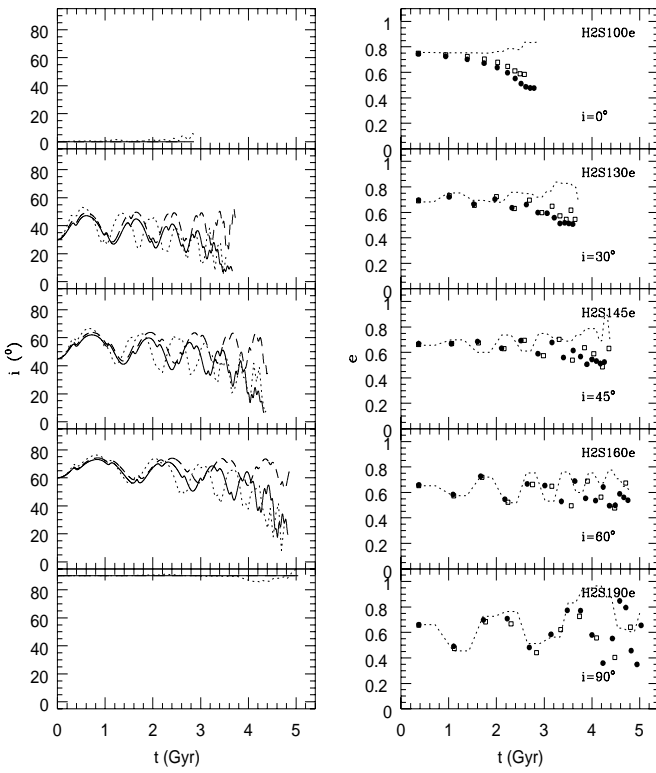


Figure 4 – continued b: As Fig. 4a for models with $e = 0.7$. Note that the time-scale has a different value.

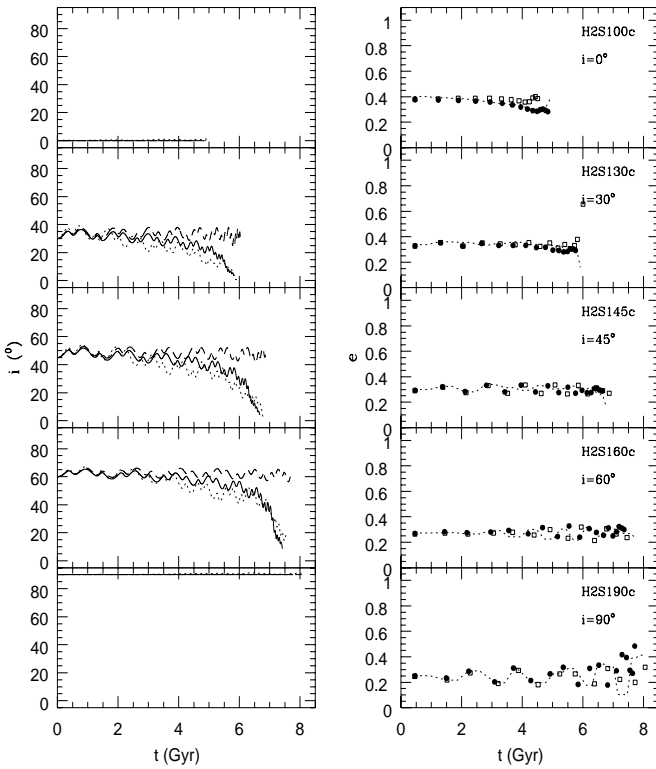


Figure 4 – continued c: As Fig. 4a for models with initially $e = 0.3$. Note that the time-scale has been rescaled.

lites suffer in oblate systems. This is crucial for simulating properly satellite motions and for investigating satellite distributions around spiral galaxies.

Like the orbital inclination, the eccentricity is one of the orbital parameters that can be indirectly measured from observations to determine a satellite's motion around a galaxy. In the right columns of Fig. 4 we show the comparison of the numerical eccentricity evolution with both semi-analytic approaches. The analytic formulae of dynamical friction lead to a larger eccentricity decrease, which occurs mostly at late-times of the orbit, the so-called *orbital circularisation*, and becomes stronger for low inclined orbits, those that suffer higher dynamical friction. Fig. 4b and Fig. 4c indicate that the circularisation is more pronounced if the initial orbital eccentricity is higher and decreases for more circular orbits. Both dynamical friction expressions lead to a similar eccentricity evolution for the first few orbital periods, however at late-times the eccentricity exhibits a reduction not present in the numerical calculations that can be as high as $\sim 80\%$ for low inclined satellites on highly eccentric orbits (Fig. 4b, model H2S100e).

7.4 Energy and angular momentum evolution

A flattened system possesses two analytic constants of motion, the energy and the component of the angular momentum perpendicular to the axi-symmetry plane (which we denote as L_z). The total angular momentum $L^2 = L_R^2 + L_z^2$ is, however, not constant during a satellite orbit (see e.g. Binney & Tremaine 1987), but has periodic variations that correspond to a precession and nutation of the orbital plane around the z -axis.

Since the dynamical friction force has an opposite sense with respect to the satellite velocity, it decreases the angular momentum and the energy which induces a monotonic sinking into the inner regions of the halo potential. The reduction of angular momentum, therefore, implies an increase of the binding energy (in absolute value), since the potential grows with decreasing radius. Due to the small magnitude of dynamical friction compared to the mean field force, we expect an easier comparison between numerical and semi-analytic data by the slow variation of L_z and E during the orbit.

In Fig. 5 we plot the changes of specific E and L_z due to dynamical friction for the models with $e = 0.5$. The results are equivalent to those of the radial evolution. Due to our selection of $\ln \Lambda$ as the average over those Coulomb logarithms that lead to the best fit for each particular model, Chandrasekhar's formula overestimates dynamical friction for low inclined orbits and underestimates it for highly inclined orbits. For orbits with $i < 30^\circ$, this appears as a stronger reduction of the z -component of angular momentum and, equivalently, a large increase of the binding energy. The effect is contrary for satellites with $i > 30^\circ$.

This figure illustrates how the kinetic energy of the satellite is lost via friction, being taken-up partially by halo particles and also being deposited in unbound satellite particles. At the end of the simulation the angular momentum has a null value, i.e the satellite remains in the inner most part of the galaxy.

It is interesting to note that the numerical evolution of energy and angular momentum presents small oscillations

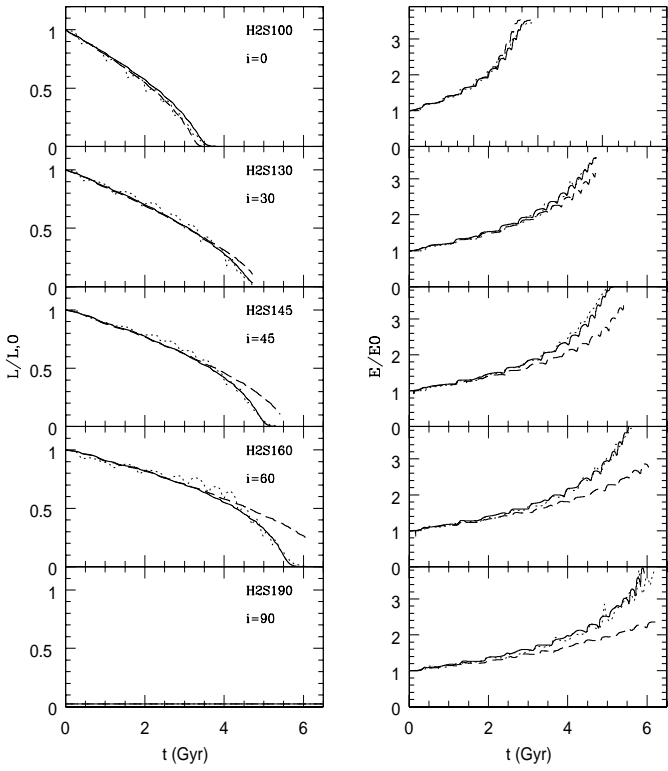


Figure 5. Specific energy and angular momentum evolution during the orbits with $e = 0.5$. The numerical evolution is denoted by dotted lines, whereas the semi-analytic data is represented by solid and dashed lines if dynamical friction is modelled by Binney's and Chandrasekhar's formulae, respectively. The quantities E and L_z are normalised to the initial value. Note that for the case $i = 90^\circ$ one has $L_z = 0$.

during the orbit. This behaviour is due to the self-response of the halo to the satellite motion. Since SUPERBOX preserves the total energy and angular momentum, the halo also moves around the centre-of-mass of the system. Due to the complexity of the feedback, it cannot be reproduced analytically (the halo centre-of-mass is fixed at the coordinate origin in the semi-analytic code).

8 CONCLUSIONS

To assess the accuracy of Binney's equations (B77) and in order to reproduce the decay of satellites in flattened DMHs with a semi-analytical code, we have performed a set of self-consistent numerical experiments for different orbital inclinations and eccentricities of the satellite. The semi-analytic code incorporates dynamical friction either in terms of Chandrasekhar's expression or as Binney's formulae. Both treatments include the aspherical density profile by means of the local approximation. This means that the differences on the satellite motion induced by each treatment of dynamical friction comes from the anisotropy in velocity space, which is implemented in the analysis of B77.

The accuracy of Binney's and Chandrasekhar's formulae in comparison with the numerical orbits is determined by the parameter $\chi^2 = \frac{1}{2k} \sum (\Delta \mathbf{r}^2 + \sigma^2 \Delta t^2)$ at the peri- and

apo-centres for a given number k of orbits. If dynamical friction is modelled by Binney's equation, this quantity shows discrepancies of approximately $\chi_{\min} = 0.009r_0$ per orbit after averaging over the set of experiments and for the first three orbits, while Chandrasekhar's formula produces values of around $\chi = 0.05r_0$ per orbit (Table 3).

We conclude that Binney's expression faithfully reproduces the process of dynamical friction in anisotropic systems. The fit is as accurate as that employing Chandrasekhar's formula in isotropic systems (see Just & Peñarrubia 2002).

The comparison of orbits resulting from Chandrasekhar's and Binney's expression of dynamical friction gives us the possibility to assess the effects of the DMH velocity anisotropy on satellite dynamics. We have demonstrated that, (i) if the density profile is in both equations $\rho = \rho(R, z)$, where R, z are the cylindrical coordinates of the satellite position vector, the orbits generated by Chandrasekhar's formula overestimate the decay time for polar orbits and underestimate it for coplanar ones for an overall best-fit Coulomb logarithm ($\ln \Lambda = 2.2$). One effect of the velocity anisotropy is then to reduce the interval of decay times as a function of the orbital inclination. Binney's expression has been shown to reproduce accurately the numerical results independently of the initial eccentricity and with $\ln \Lambda = 2.4$. (ii) Dynamical friction in systems with anisotropic velocity distribution leads to a marked decrease of the orbital inclination i which is well reproduced by Binney's expression. After the satellite sinks to the innermost region of the galaxy, i lies within $10-20^\circ$, independently of the initial value unless $i \approx 90^\circ$ (polar orbits). (iii) The energy and angular momentum evolution as a function of the orbital inclination confirm the results of (i) and (ii).

The semi-analytic eccentricity evolution, either employing Chandrasekhar's or Binney's formula, shows the so-called *circularisation* process, defined as the progressive reduction of e during the orbit. This variation is stronger for increasing friction (as for coplanar orbits or during the late-times of the evolution) and barely takes place in the self-consistent N -body calculations. The small N -body circularisation agrees with the results of van den Bosch et al. (1999). A possible solution may be sought in the position-dependence of the Coulomb logarithm, as proposed by Hashimoto, Funato & Makino (2003). However, despite the improvement in the description of the orbit at early-times, the scheme of Hashimoto et al. overestimates the satellite decay time for all the experiments (see Just & Peñarrubia 2002). We must conclude that the reason for circularisation in the semi-analytic orbits is not yet fully understood.

9 ACKNOWLEDGEMENTS

JP acknowledges support through a SFB 439 grant at the University of Heidelberg. PK acknowledges support through DFG grant KRI635/4. We thank the anonymous referee for his/her advice and useful comments.

REFERENCES

Arnaboldi M., Capaccioli M., Cappellaro E., Held E.V., Sparke L.S., 1993, *A&A*, 267, 21

Bahcall N., Ostriker J.P., Peltz P., Steinhardt P.J., *Science*, 284, 1481

Becquaert J.F., Combes F., Viallefond F., 1997, *A&A*, 325, 41

Binggeli B., Sandage A., Tarenghi M., 1984, *AJ*, 89, 64

Binney J., 1977, *MNRAS*, 181, 735 (B77)

Binney J., Tremaine S., 1987, *Galactic Dynamics*. Princeton University Press, Princeton, New Jersey

Boily C.M., Kroupa P., Peñarrubia J., 2001, *NewA*, 6, 27

Boute D.A., Canizares C.R., 1998, *ApJ*, 468, 184

Bullock J.S., 2001, *astro-ph/0106380*

Chandrasekhar S., 1943, *ApJ*, 97, 255

Chandrasekhar S., 1960, *Principles of Stellar Dynamics*. Dover, New York

Colpi M., Mayer L., Governato F., 1999, *ApJ*, 525, 720

Del Popolo A., 2003, *A&A*, 406, 1

Del Popolo A., Gambera M., 1998, *A&A*, 342, 34

Dubinsky J., 1994, *ApJ*, 431, 617

Fellhauer M., Kroupa P., Baumgardt H., Bien R., Boily C. M., Spurzem R., Wassmer N., 2000, *NewA*, 5, 305

Hashimoto Y., Funato Y., Makino J., 2003, *ApJ*, 582, 196

Hofner P., Sparke L., 1994, *ApJ*, 428, 466

Holmberg E., 1969, *Arkiv. Astr.*, 5, 305

Ibata R., Lewis G.F., Irwin M., Totten E., Quinn T., 2001, *ApJ*, 551, 294

Johnston K.V., Sigurdsson S., Hernquist L., 1999, *MNRAS*, 302, 771

Just A., Peñarrubia J., 2002, *A&A*, submitted; ARI-Preprint 110

King I.R., 1966, *AJ*, 71, 65

Klessen R.S., Kroupa P., 1998, *ApJ*, 498, 143

Kroupa P., 1997, *NewA*, 2, 139

Law D.R., Majewski S.R., Johnston K.V., Skrutskie M.F., *astro-ph/0309567*

Maoz E., 1993, *MNRAS*, 263, 75

Olling R.P., 1996, *AJ*, 112, 481

Olling R.P., Merrifield M.R., 2000, *MNRAS*, 311, 361

Peebles P.J.E., 1993, 'Principles of Physical Cosmology', Princeton University Press, Princeton

Peñarrubia J., Kroupa P., Boily C.M., 2001, *MNRAS*, 333, 779 (PKB)

Peñarrubia J., 2003, PhD Thesis, Universität Heidelberg, Germany. <http://www.ub.uni-heidelberg.de/archiv/3434>

Pfenniger D., Combes F., Martinet L., 1994, *A&A*, 285, 79

Press W.P., Flannery B.P., Teukolsky S.A., Vetterling W.T., 1986, *Numerical Recipes*. Cambridge University Press, New York

Prada F. et al., 2003, *ApJ*, 598, 260

Prugniel Ph., Combes F., 1992, *A&A*, 259, 25

Sales L., Lambas D.G., 2003, *astro-ph/0311432*

Sciama D., 1990, *MNRAS*, 244, 1

Statler T.S., 1991, *ApJ*, 375, 544

Steinman-Cameron T.Y., Kormendy J., Durisen R.H., 1992, *AJ*, 104, 1339

Taylor J.E., Babul A., 2001, *ApJ*, 559, 716

Udry S., Martinet L., 1994, *A&A*, 281, 314

van den Bosch F., Lewis, G.F., Lake G., Stadel J., 1999, *ApJ*, 515, 50

Velázquez H., White S.D.M., 1999, *MNRAS*, 304, 254

Whade M., Donner K.J., 1996, *A&A*, 312, 431

Zaritsky D., González A., *PASP*, 111, 1508